WORCESTER POLYTECHNIC INSTITUTE

Ocean Wave Energy Harvesting

Off-Shore Overtopping Design

Steven Como, Jan Keleher, Passe Meas, Kelsey Stergiou and Jessica Williams

3/1/2015

Abstract

Renewable energy is a topic that is constantly discussed in the scientific world, for many of the energy sources that are used daily are in short supply. As the ocean makes up 70% of the Earth, wave energy as a renewable source is an option that could potentially bring a large amount of energy with the proper processes. In order to address this, many current wave-capturing mechanisms were researched to determine the most ideal project for college students to develop further. A device and test tank were constructed and results were obtained by using a variety of wave heights to attempt a small sampling of the waves that the device would encounter in open deep-water ocean. With a scaled down model, the device captured 13.4 L of water over 60 waves, resulting in 0.34 kW/m of power for the scaled-up model. These results compare to similar devices in this way.

Table of Contents

Table of Figures

Table of Tables

Chapter 1 – Introduction

The population is well aware of the energy crisis that cannot be averted without making progress in the way of clean, renewable energy sources. Due to the high potential of ocean waves, wave energy harvesting is an industry with a constant flux of emerging start-up companies innovating ideas to capture this energy. Waves are a natural, renewable, free source of energy, providing an ideal alternative to other detrimental sources because the collection and redistribution of waves allows for endless energy harvesting. Many approaches have been attempted in converting wave energy into electricity with successful defining features being cost efficiency, safety, and reliability. There are eight main types of energy converter machines, but just one, overtopping devices, will be focused on for this project. Overtopping devices collect ocean waves in an above-water reservoir and then discharge the water into the ocean by means of turbines. Wave Dragon is an example of this type of device that gathers waves by means of two long arms that direct water into a central reservoir and then releases it once it has gone through the turbines. The Seawave Slot-cone Generator utilizes tiered reservoirs to amass more of the wave without using arms to reroute it. Within this project, a three-tiered overtopping device was developed to collect waves of differing heights within a motorized wave tank that would simulate deep-water waves. The deep-water aspect of the device appeals to the aesthetic dimension, for a coastal collection overtopping device hampers the view from beaches or coastlines. It can also upset fishing locations and habitats of a variety of sea creatures. This device was a combination of many ideal characteristics of other researched wave harvesting devices, including the tiers and turbines to amass the waves and produce power. Many calculations were deliberated to discover the ideal scaling factor, the proper cam dimensions, and motor parameters. The purpose of this project was to develop a device that was comparable to current devices in the field.

Chapter 2 – Background

2.1 Why Renewable Ocean Energy?

The need for additional energy to sustain the growing population of the world calls for better and more innovative technologies. Many current technologies include nuclear power or biofuels, which have been linked to environmental concerns. Ocean energy harvesting devices were first displayed in 2008 with an array of designs, including floating wind turbines, as well as tidal, wave, and thermal energy converters (Esteban, 2012). Clean, renewable energy harvesting is preferred over nuclear or biofuel-powered plants, but many renewable sources are unable to be operated on a large-scale. In order to find a way to implement large-scale operation, different designs are continuously being researched and developed.

2.2 Why Waves?

The advantages of wave energy harvesters outnumber the advantages of other ocean energy harvesting methods such as tidal power, ocean thermal energy conversion (OTEC), and saline mechanisms. Waves are abundant in all areas throughout the ocean, making them more useful in energy harvesting than tides. Although tides have the potential to generate large amounts of power (approximately 3,000 GW worldwide) less than 3% of areas are suitable to actually harness tidal power (Esteban, 2012). Tides are predictable and consistent; however, due to the limited abundance of locations, tidal power is difficult to incorporate on a large scale. Alternatively, waves are not as easy to predict, but they are found in many more locations throughout the world, as can be seen in Figure 1.

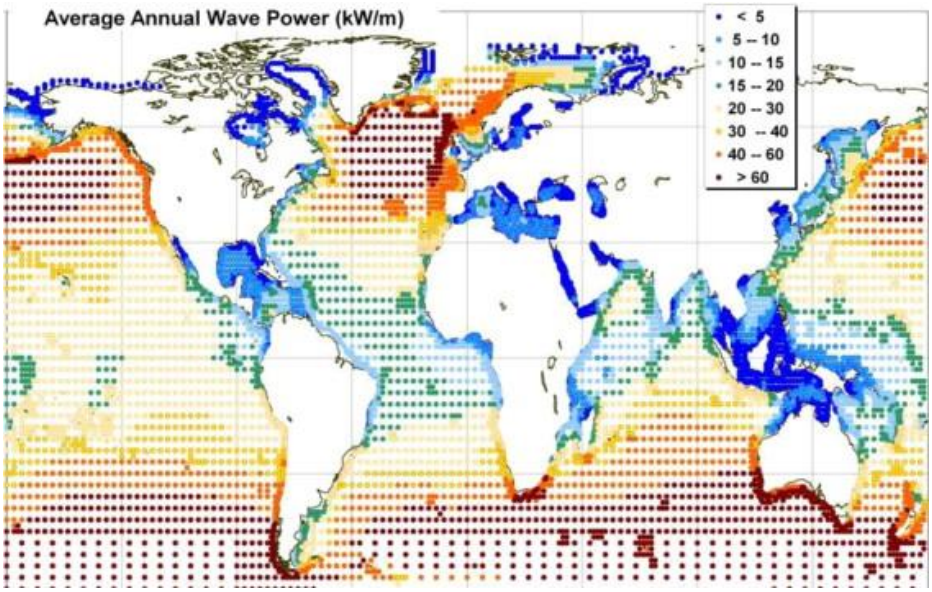

Figure 1: Map of Wave Power Potential Throughout the World (Alamian, 2014)

The map shows that there is high wave power potential in widespread areas, especially those further from the equator. Wave energy has been estimated to have the potential to produce 1,000-10,000 GW of power, which is close to the world electrical energy consumption (Esteban, 2012). From this information, it can be argued that wave energy harvesting is more accessible than tidal energy harvesting.

Another form of ocean energy harvesting is by OTEC mechanisms. OTEC utilizes the ocean's natural absorption of solar energy to produce power. As the heat of the sun warms the surface of the water more than the greater depths, a temperature gradient is created. The temperature of the surface water will vaporize a fluid with a low-boiling point, which will then expand into gas and spin a turbine. This turbine is connected to a generator, which produces electricity. Cooler seawater is brought in by a pump that cools the vapor back into a liquid so it can be continuously reused in the cycle. The larger the temperature differential, the higher the efficiency of the cycle; therefore, ideal locations for this technology include waters around the Equator (Esteban, 2012). The limitation of location provides evidence why waves are a more accessible and favorable option in the field of ocean energy harvesting.

Prototype saline mechanisms harvest energy from bodies of water where both fresh and salt water are present, such as estuaries. The mechanism divides the water types by means of a semipermeable membrane. The osmosis that occurs as the fresh water moves across the gradient of higher salinity to dilute the solution increases pressure. Once the system reaches a certain pressure, achieving a high enough head, it will spin a turbine and generate power (Lockwood, 2013). The complexity of this mechanism, along with the limitations in location, make saline energy converters less feasible than wave energy converters.

Although a number of renewable energy sources are undergoing research, wave energy harvesting provides advantages over other competitive methods. One major advantage is the wide span of locations in which waves can be captured. Devices can be incorporated in the open ocean where high energy waves are present or along the coastline to minimize construction and maintenance costs. Additionally, unlike solar energy, waves can be continuously collected at all hours of the day and night. In addition to the versatility in location and collection times, waves are produced year round and are a source of free energy. A major benefit of wave converter devices, in comparison to wind farms, power plants, and other power production sites such as the Alaskan pipeline, is their minimal use of land. There are numerous advantages to using different forms of alternative energy; however, wave power is a compelling source for energy production.

In order to understand how to extract power from waves, it is essential to first understand the mechanism of how waves work. Waves are created by the force of wind on open water. As the force of the wind reaches the surface of the water, waves are produced. These waves then travel, containing high amounts of energy, until they reach an area of shallow depth, usually a beach. At this point, waves begin to lose energy due to frictional losses at the seabed surface. The wavelengths shorten, speeds are reduced, and the wave profile steepens, resulting in the "breaking" of the wave (Tester, 2012). Due to this loss of energy, waves in open water have much higher energies than waves that are found along coastal regions.

All waves have potential energy that can be transformed to power through use of wave energy converters. Waves that are far offshore exhibit higher potential energy than waves that are found near the shoreline by about 10% (Thurman, 2001). The potential energy of a wave can be calculated by the following equation:

$$\Delta PE = \frac{1}{16}\rho\lambda g h^2$$

In this equation, the potential energy only accounts for two dimensions, meaning that this is the potential energy per width of the wave. The variables in the above equation represent:

$$\rho = density\ of\ the\ water\ \left(1025\frac{kg}{m^3}\ for\ seawater\right)$$

$$g = acceleration\ of\ gravity\ (9.81\frac{m}{s^2})$$

$$h = crest - to - trough\ wave\ height\ (about\ 2m)$$

$$\lambda = wavelength$$

The wavelength can be described as:

$$\lambda = \frac{gT^2}{2\pi}$$

Where:

$$T = wave\ period\ (approximately\ 5 - 10s)$$

The potential energy of the wave can then be converted to power by dividing the potential energy by the time period. This results in the following equation for power:

$$P = \frac{1}{32\pi}\rho g^2 h^2 T$$

Substituting the density of seawater (1025 kg/m^3) and acceleration due to gravity (9.81 m/s^s) into the equation, it can be reduced to:

$$P = 0.98h^2T$$

The units for this power equation are kW/m, meaning that it would be the power output per unit width. A schematic of a wave is shown in Figure 2.

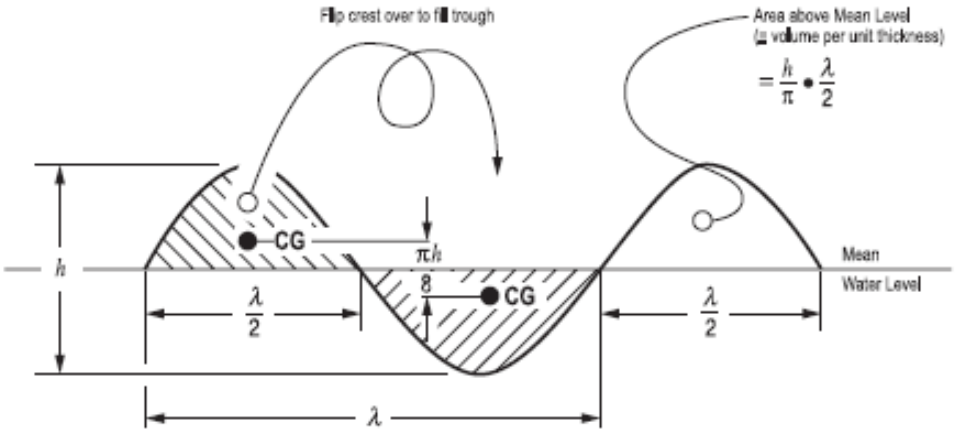

Figure 2: Schematic Deriving Potential Energy and Power of a Wave (Tester, 2012)

This schematic includes variables that are used to derive the potential energy and power equations for a wave. From this, one can better understand the mechanics of a wave and therefore predict the power output for a wave energy converter.

2.3 Types of Wave Energy Harvesting

There are numerous devices that have been established in the wave energy industry that attempt to most efficiently convert the potential energy of waves into power. The four primary categories of wave energy converters (WECs) are: point absorbers, attenuators, oscillating water columns, and overtopping devices. Each of these WECs has different attributes, giving them varying advantages and disadvantages.

Point absorbers, seen in Figure 3, are the simplest WECs. These devices float on the surface of the water and generate energy through the periodic passing of waves which causes the device to bob up and down. Point absorbers depend on an internal hydraulic system that pumps air to power a generator as the cylinder is compressed and released by wave energy. They rely on the frequency of waves to generate electricity, and can attain maximum energy absorption by matching the optimal frequency and wave height (Voorhis, 2012). The disadvantages of point absorbers are their inability to adapt to the varying height and frequency of waves, which prevents optimization through consistency. Additionally, large waves produced by storms significantly reduce the efficiency of these devices and can even damage them if they are too forceful.

Figure 3: Point Absorber Device (Voorhis, 2012)

Attenuators are long, cylindrical, segmented structures that float on the surface of the water, operating in parallel with the roll of the waves, much like the motion of a ship. The segmented regions allow for these cylinders to bob in the water due to passing waves which drive the hydraulics of the device similar to that of point absorbers. The difference between attenuators and point absorbers rests primarily in the relative size of the structures. The mechanics of the two systems operate on similar basic principles of hydraulics driven by periodic wave frequencies; however, the attenuators are able to capture a wider range of waves due to their large size. Additionally, attenuators are more rugged and can survive harsh storms that generate greater waves as can be seen in Figure 4 below.

Figure 4: Wave Attenuator Device (Pelamis, 2012)

Oscillating water columns operate based on a pressure differential created between air and the ocean water within a structure that is half submerged in the water. These columns are constructed

along the shoreline to capture waves crashing on the coast, utilizing the wave pressure to push air through a hollow cavity that is attached to a turbine. The rapid decrease in water pressure then pulls air back through the bi-directional turbine, generating electricity through air flow in both directions. This structure provides a simple, sturdy design that is able to convert wave energy at low maintenance costs due to the lack of complex internal machines. An example of an oscillating water column can be seen in Figure 5 below.

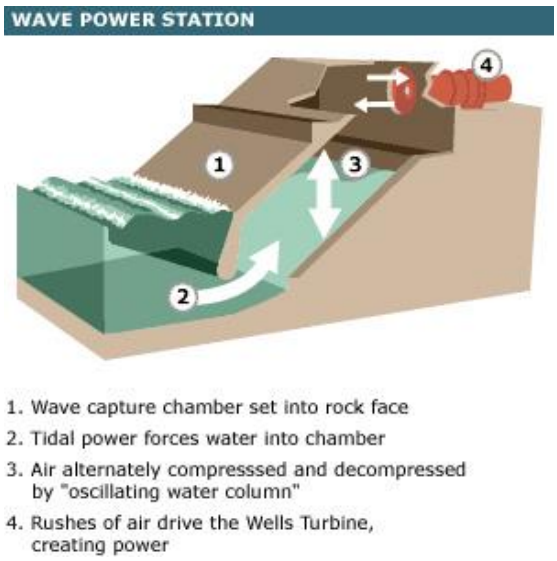

Figure 5: Oscillating Water Column (Emay, 2010)

Lastly, overtopping devices function based on a pressure differential created between an artificial reservoir and the surrounding ocean water. The basic design of overtopping devices involves a ramp leading up to a reservoir with a retaining wall. Potential energy is then converted into power through turbines that are located in the bottom of the reservoir as shown in Figure 6. By building up the water level inside the reservoir from waves crashing over the ramp, a pressure gradient is created due to an increase in pressure inside the reservoir, resulting in the flow of water through the turbines. Compared to oscillating water columns, this straightforward, robust design provides a means for capturing a large volume of waves and generating electricity without the use of internal mechanisms, therefore minimizing the cost of maintenance and repair.

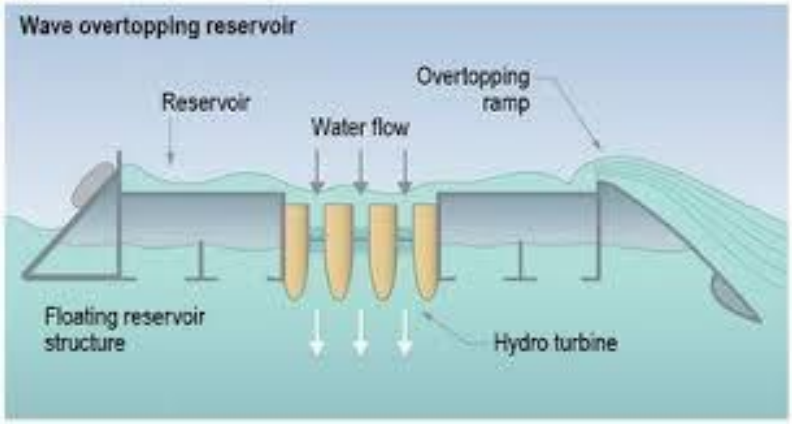

Figure 6: Overtopping Device (Bedard, 2005)

2.4 Overtopping Design Combination

By researching various methods in wave energy conversion, a new device that combines the advantages of overtopping with a multi-tiered system was conceptualized. With a rapidly expanding market for WECs, numerous innovations exist; however, there is great potential to create more efficient designs to produce free energy. Combining ideas from two pre-existing designs, the Seawave Slot-cone Generator and Wave Dragon, a new overtopping system can be created.

The Seawave Slot-cone Generator (SSG) is an overtopping device that was created by WAVEenergy in Norway. It entails a number of stacked reservoirs that store the energy of collected waves as potential energy until it can be converted into electricity through a multi-stage turbine. Compared to similar water collection devices, the SSG has added effectiveness due to its multiple reservoirs, higher cost-efficiency due to incorporation into pre-existing structures, water recirculation, and easy installation/maintenance due to the fact that no cables or moorings need to be mounted underwater. A disadvantage of the SSG falls within its location. Since it is used along the coast, the size of the waves that it encounters is smaller and therefore less powerful than those of systems that are installed offshore. In terms of economic and technical dilemmas, there have been some questions related to the protection of harbors if the SSG is assimilated into pre-existing structures (Vicinanza, 2012).

Erik Friis-Madsen and Wave Dragon Ltd. invented and developed the Wave Dragon, which is an overtopping device that floats on top of the water and collects waves by means of two large arms, known as wave reflectors. These reflectors direct waves towards a ramp where they crash into a reservoir. The water is then briefly stored before leaving the reservoir through Kaplan turbines located at the bottom. Kaplan turbines are usually used in hydropower plants as they produce electricity from hydraulic head. The water is returned to the ocean after it runs through the turbines and this constant

cycle creates a clean source of energy that can be reused indefinitely. “Wave Dragon is currently the largest device – by rated power and physical dimensions – under development” (Wave Dragon, 2006). In 2003, the first power-collecting prototype of Wave Dragon was set up at Nissum Bredning, which is off the coast of Denmark. The energy production of this device is constant, its annual energy output is about 619 MWh, has a capacity factor of approximately 20%, and can be downsized to collect the energy from smaller waves as well. Wave Dragon is unable to produce electricity from waves with heights of less than 1 m, as well as in cases with overly large waves, such as a tropical storm or a tsunami. The device is designed to handle “energetic wave climates”, which is defined as areas where the wave power is 50 kW/m or higher (Wave Dragon, 2006).

Combining the onshore, multi-tiered, SSG with the popular Wave Dragon provides a wide range of benefits to improve the power output of the design. A primary advantage of utilizing the open ocean versus a shoreline device is the difference in energy capacity for the characteristic waves. Open ocean waves contain approximately 10% more power than shoreline waves due to the frictional losses of the ocean floor. These losses act on waves shallower than one half of the wavelength deep, which is the case for the majority of waves crashing on shore. The effective depth of the wave is equal to about one half of the wavelength and, therefore, in shallow waters, the ocean floor actually opposes wave movement, reducing the overall energy of the wave (Vicinanza, 2012).

A major downfall of the Wave Dragon design can be attributed to the limited capture of waves at specific heights dependent on the ramp of the device. The Wave Dragon has a set height for the ramp, reservoir, and external walls, whereas the multi-tiered on-shore device captures waves at varying heights. Potential energy relies on the height at which the wave is captured and is maximized at the highest point of the wave. By capturing the wave at its tallest height, the maximum volume of the wave may be collected by the system. Since the system can also accept waves shorter than the maximum height, the conceptual combined design optimizes the heights and volumes of capture for improved potential energy to be stored by the reservoirs.

Furthermore, the reservoir draining of the Wave Dragon produces additional inefficiencies by starting and stopping the turbines in the system as each cycle of water empties out. By using a multi-tiered system, there is a higher possibility of maintaining a larger volume of water in the reservoirs to establish constant flow through the turbines, which will significantly improve the efficiency of the system by drastically reducing frictional losses in the turbines. This reduction in losses results from preventing the stopping and starting inefficiencies of the turbines from occurring at each wave cycle and keeping the turbines in constant motion. Since the multi-tiered system captures waves at different

levels and fills multiple reservoirs, the water takes longer to drain through the system, thus providing constant flow to keep the turbines spinning.

Chapter 3 - Methodology

The goal of this project was to test the efficiency of combining two overtopping designs, Wave Dragon and SSG, into one wave energy harvesting device. To achieve this goal, the following objectives were completed:

1. Conducted research on Wave Dragon and SeawaveSlot-cone Generator to determine which characteristics are most favorable at producing high wave energy efficiencies.
2. Used proper scaling factors to determine reasonable testing conditions.
3. Researched, developed, and designed a wave generation system that produced necessary testing environment.
4. Designed a model within Solidworks of the intended overtopping device.
5. Constructed the test tank and wave energy converter.
6. Performed testing and gathered data on the power output of the new device.
7. Analyzed the power produced by the device.

This chapter contains descriptions of the objectives and methods used throughout the process that enabled the completion of the overall goal: testing the efficiency of combing two overtopping designs.

3.1 Existing Designs

In order to develop a new overtopping device, existing designs were first explored. Two designs that exhibited high potential in the field of wave energy harvesting included Wave Dragon and SSG as discussed in Chapter 2. By combining the multiple reservoirs of SSG with the offshore aspect of Wave Dragon, the concept of a device that exhibits superior wave power generation was fashioned.

3.2 Scaling Factors

In order to create a functional scale model of the wave energy converter designed for this project, it was important to evaluate the feasibility of the presented design. Calculations of Froude scaling factors, power calculations, and varying wave factors all contributed to the overall capacity of the design. Assumptions needed to be made regarding inefficiencies and losses that would be encountered during testing. These assumptions included the percentage of wave volume captured, efficiency of the turbines, and the efficiency of the generator. Considering the different inefficiencies and assumptions of the wave converter system, preliminary calculations gave more tangible parameters for the device as well as potential room for improvement.

3.2.1. Assumptions

There are a number of assumptions to be considered when analyzing any power system. Losses in the system are a common assumption made in a real situation as frictional effects and inefficiencies will be produced by the turbines, generators, fluid flow, and wave capture of the device. To simplify the prototype, a turbine and generator were omitted; but for this project's calculations, the effective efficiency of these devices were considered when determining the overall power output of the system. Researching current technology, revealed turbine and generator efficiencies of 85% and 95%, respectively. Additional losses in energy while the waves enter the system can be determined by the Reynold's and Froude numbers associated with the device. For scaling purposes, it is impossible to scale both of these dimensionless constants equally; therefore, the Froude number was used to scale the fluid flow conditions. Froude scaling calculations relate the model to the full scale device by accounting for the loss in wave energy due to the flow conditions of the wave as they enter the wave converter device. The combination of all of these assumptions provides a baseline for preliminary power calculations that the designed system can expect to produce.

Furthermore, when waves travel up the ramp and into the reservoirs, the entirety of the wave will not be captured. For purposes of simplification, it was assumed that 75% of any given wave volume will be captured by the device. Realistically, this value will change for each wave dependent on the wave height and other wave characteristics, however, the wave capture volume is assumed to be 75%. In relation to wave volume captured, the "felt" wave height is important since waves do not solely act above the water. Research shows that the "felt" wave height extends approximately half of the wavelength below the surface of the water (Thurman, 2012). Considering this assumption is vital to the design of the system to assure that the test tank is deep enough to enable free movement of the effective depth of the wave. Assuming deep waves as opposed to shallow waves more accurately depicts the system on the open ocean because it neglects frictional losses of the ocean floor. Removing these frictional losses provides an advantage over a shoreline system.

Considering the effects of the shoreline friction on waves, the wave height was estimated using the water height based on the assumption that the "felt" wave depth extends by half of the wavelength under the surface. The wavelength was assumed to be seven times the chosen wave height as is the average characteristic of a general wave system (Thurman, 2012). Therefore, the overall height of the waves "felt" by the system was estimated to be seven times the height to determine average wavelength, divided by two since this is the depth below the water that the wave still impacts. Based on

the wave height and wavelength assumptions the maximum wave height able to be produced for the given system can be modeled by the following function:

$$h_{wave} = \frac{2}{7} * h_{water}$$

Where h_{wave} is wave height and h_{water} is the water height. Using the above equation prevents frictional losses from the bottom of the test tank to better simulate open ocean waves. Therefore the tested maximum wave height, based on a water height of 12 inches is:

$$h_{wave} = \frac{2}{7} * 12\ inches = 3.43\ inches = 8.70cm$$

3.2.2. Froude Scaling Factor

The Froude number is an important dimensionless group to be taken into consideration when designing a system that involves wave production. Froude scaling is beneficial since the Reynolds number is a more difficult factor to scale. “If Re is to be kept constant, the value of U (velocity) at model scale has to be 100 times that of the full-scale value. The obvious way to overcome these conflicting requirements would to be increase g and/or decrease v (viscosity)” (Payne, 6). In order to achieve these conditions, a centrifuge or vacuum chamber would be required for testing. Seeing as both are unfeasible within an undergraduate project constraint, maintaining a constant Reynolds number had to be abandoned in favor of using Froude scaling factors.

Froude scaling is much easier than Reynolds scaling. Assuming that the force of gravity and viscosity remains the same, the forward speed of the fluid at model scale has to be 1/10th of the full scale one (Payne, 6). The Froude number is a dimensionless value that represents the free surface flow regime of water when waves are formed. If this value is less than one, the state of the flow is subcritical, if this value is equal to one, the state of the water is critical, and if this value is greater than one, the state of the water is supercritical. This flow assumption is comparable to that predicted by the Reynolds number calculation. At supercritical levels of flow, high turbulence will contribute to significant power losses from the system. For this reason it is imperative to keep minimized frictional factors in mind for design intent of the wave converter. The Froude number is a strong representation of flow in a wave converter system because the hydraulic jump experienced by the ramp can be modeled to accurately represent mechanical losses. This factor is easier to scale than the Reynolds number because it is dependent on the ramp which has been designed to minimize losses. Since it is necessary to choose a scaling factor that will most accurately be modelled by the designed environment, the Froude scaling method has been used for the system, derived by the equations found in **Error! Reference source not**

found. below. “For many tank-scale wave energy converters, the net influence of viscous forces on body motions are small and Froude scaling can be assumed to be satisfied” (Payne, 6).

Table 1: Froude Scaling Factors (Payne, 2008)

Quantity	Scaling
wave height and length	s
wave period	$s^{0.5}$
wave frequency	$s^{-0.5}$
power density	$s^{2.5}$
linear displacement	s
angular displacement	1
linear velocity	$s^{0.5}$
angular velocity	$s^{-0.5}$
linear acceleration	1
angular acceleration	s^{-1}
mass	s^3
force	s^3
torque	s^4
power	$s^{3.5}$
linear stiffness	s^2
angular stiffness	s^4
linear damping	$s^{2.5}$
angular damping	$s^{4.5}$

The various scaling factors account for the wave conditions that are kept constant for any scaled system. The assumptions made to calculate the desired wave conditions were determined by the Froude scaling factors. The table can be used to determine a wave period and frequency based on the wave height derived for the system. Additionally, the mass of the waves captured and the power potential of the waves can be estimated by these scaling factors.

Given the wave height of 3.43 inches (8.70 cm), the wave period can be scaled appropriately by the Froude scaling factor of $s^{.5}$, where s is equal to the wave height. Therefore, the scaling factor for the period associated with the given wave height for the scaled system is:

$$s_T = s^{.5} = .087^{.5} = .295$$

Where s_T is the Froude scaling factor for the wave period given a wave height of 3.43 inches. Multiplying this scale factor by an average period of ground swell waves, which characterize the waves acting at the ocean depth of the device’s location, yields:

$$T = s_T * 9s = .295 * 9s = 2.66s$$

Where T is the scaled period of the waves given a 3.43 in wave height and 9s as the average period for ground swell waves for a full-scale system. Therefore a reasonable scale for the wave period based on a 9 second ground swell period is approximately 3 seconds.

Using a similar method, the mass and power potential for each wave can be estimated based on the various Froude scaling factors that are derived from the table above. The mass of each wave captured by the wave converter can be estimated by:

$$s_m = s^3 = .087^3 = .00066$$

Where s_m is the Froude scaling factor for the mass of each wave for the 3.43 inch wave height produced. To find the actual mass captured by each wave, the scaling factor can be multiplied by the estimated mass for a full scale system.

Finally, the same method can be utilized substituting the s^3 with $s^{3.5}$ to estimate the power of the scaled system based on the full size system. The power scaling coefficient will then be calculated by:

$$s_P = s^{3.5} = .087^{3.5} = .00019$$

Where s_p is the Froude scaling factor for the power potential of each wave for the same 3.43 inch wave height. Again, the actual power potential for each wave for the scaled system can be achieved by multiplying this scaling factor by the estimated power in a life sized system.

Froude scaling factors can be used for a variety of assumptions by just defining a wave height. In using these scaling factors, the accuracy of the power calculations can be determined. These values can be further compared to experimental data to estimate losses for the designed system.

3.2.3. Power Calculations

In order to ensure the feasibility of the device, it was necessary to complete some of the background theoretical power calculations. These calculations involve the scaling factors derived above, the specific design of our wave capture device, and the volume and potential energy of water in the reservoirs.

The new design uses three separate tiers to capture water. This is important as the higher the water can reach, the more potential energy the volume of water contains, and as a result, the more kinetic energy can be extracted from the water. Due to the shape of each wave (the wavelength being approximately 7 times the height of the wave), the first tier is designed to capture as much water as possible from the lower part of the wave. The second and third tiers are designed to maximize their relative reservoir height. All the reservoirs and tiers are lipped such that any water that does not make it to the top of the second or third tier will simply flow down to the tier below it.

In addition, the tiers achieve a maximum height equal to 1.2 times the average wave height. This allows for the maximum capture of over 95% of waves, and allows for the device to utilize the forward kinetic energy of the waves to bring them up the ramp, to a higher reservoir, maximizing potential energy. The schematic in Figure 7 shows how the wave is split into three tiers correlating it to the three tiers of the device.

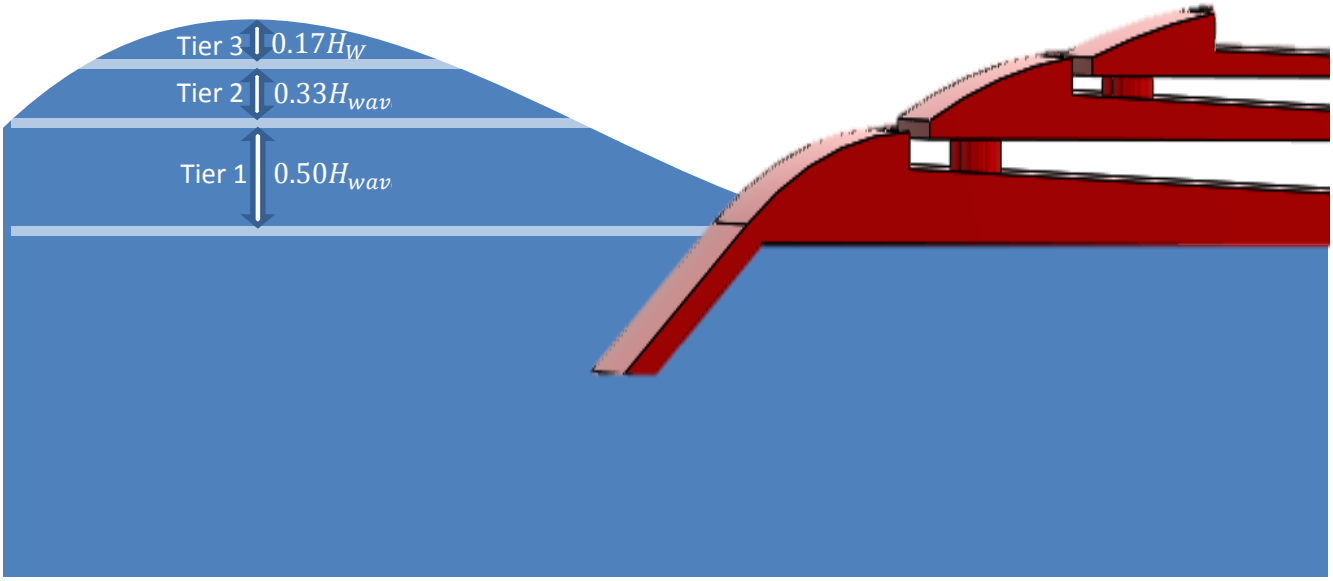

Figure 7: Schematic of Device

From calculations using Froude number and appropriate scaling, it was determined that the simulation tank, containing a water depth of 12 inches (or 0.3048 meters), is able to produce 3.43 inch waves. Using 3.43 inch simulated waves, estimation of the wave collection capacity and the power output of the testing device can be determined.

$$Wavelength\ of\ Wave = \lambda = 7h$$

$$Area\ of\ a\ Wave = \frac{h}{\pi} * \frac{\lambda}{2} = \frac{h}{\pi} * \frac{7h}{2} = \mathbf{\frac{7h^2}{2\pi}}$$

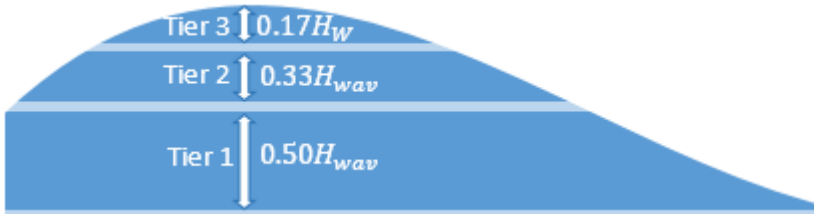

Figure 8: Wave Capture Schematic

$$Area\ of\ Tier\ 3 = T_3 = \frac{h\,\lambda}{2\pi} = \frac{7h^2}{2\pi} = \frac{7\frac{\boldsymbol{h}^2}{\mathbf{6}}}{\mathbf{2\pi}} = \mathbf{2.18\ in^2}$$

$$Area\ of\ Tier\ 2 = T_2 = \frac{h\,\lambda}{2\pi} - T_3 = \frac{7h^2}{2\pi} - T_3 = \frac{7\frac{\boldsymbol{h^2}}{\boldsymbol{2}}}{\boldsymbol{2\pi}} - \boldsymbol{T_3} = \boldsymbol{4.37\ in^2}$$

$$Area\ of\ Tier\ 1 = T_1 = \frac{h\,\lambda}{2\pi} - T_2 - T_3 = \frac{7h^2}{2\pi} - T_2 - T_3 = \frac{\boldsymbol{7(h^2)}}{\boldsymbol{2\pi}}\boldsymbol{(0.75)} - \boldsymbol{T_2} - \boldsymbol{T_3} = \boldsymbol{6.56\ in^2}$$

Table 2: Constant Variables

Constant Variables	
Period (T) (s)	3
Gravity (g) (m/s^2)	9.81
Density (ρ) (kg/m^2)	1025
Wave Capture Efficiency	75 %
Tier 1 Relative Height	0.6h
Tier 2 Relative Height	1.0h
Tier 3 Relative Height	1.2h

Calculations of volume, energy and power values are "per inch" for the width of the device. Instead of considering the volume of each wave, the area of each wave (or volume per inch) will be considered. In addition, most of the calculations will remain as per wave values. The total captured volume (per inch), is a summation of the volume captured in each tier.

$$Total\ \frac{Volume}{inch}of\ All\ Tiers = T_T = 13.11\ in^2$$

From the volume captured in each reservoir height, we can extract the potential energy stored in each reservoir. Simply put:

$$PE = mgh = V\rho gh$$

$$PE_{Total} = \rho g(V_1h_1 + V_2h_2 + V_3h_3) = 105\ Joule$$

This is per wave per inch of device structure, therefore the power output can be estimated under the assumption that the volumetric flow rate in is equal to the volumetric flow rate out. We assume that the flow rate is constant, meaning that the reservoirs are replenished every wave period of 3 seconds. As such:

$$Power = \frac{PE_{Total}}{T} = \frac{105}{3} = 35\ Watts$$

Using the scaling factor derived from the Froude Number of $s^{3.5}$, this gives us a real world output of about 44 kW per wave per meter of the device. While the theoretical power output is important to our design, just as important is the volumetric flow rate, as it will be measured through the output of the device. Our calculations estimate a volumetric flow rate of around 47 cm^3/s per meter of the device.

3.3 Development of Wave Generation System

Once the appropriate scale for the prototype and waves was determined, a wave generation system, consisting of a crank-rocker four bar mechanism, was developed in order to test the prototype. In this design, a board was hinged to the bottom of a test tank. At a desired height of the board, a rod was attached by a pin. The rod can be modeled as a two force member, with only the force of the board and the force of the other linkage acting on it. The end of the rod opposite the board is pinned to a cam that is press-fitted on a motor shaft, completing the four bar linkage. The cam acts as the crank while the board acts as the rocker. A picture of this mechanism can be seen in Figure 9.

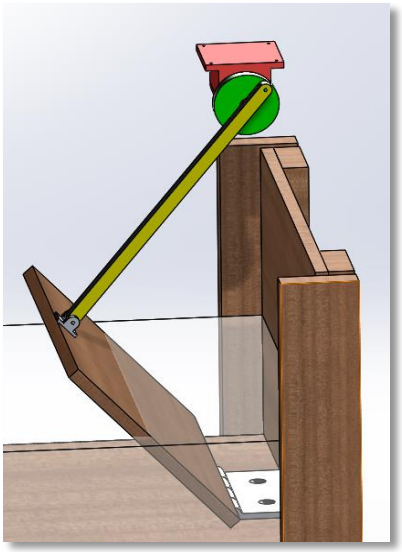

Figure 9 Wave Generation Mechanism

In order for a four bar linkage to have a link that can complete a full revolution, Grashof's condition must be satisfied. Grashof's condition states that the sum of the lengths of the shortest and longest links must be less than the sum of the lengths of the two intermediate-sized links (Natesan, 1994). In a traditional four bar linkage, there are additional limitations to the lengths of the bars to avoid locking of the mechanism, but these limits can be ignored since the crank and rocker are on two completely different planes. In this system, the concern is not centered about locking out the mechanism, but rather ensuring that the links are long enough for all ranges of movement.

As the board rocks back and forth the water is displaced, and waves are created. The height of the waves and the frequency of wave production can be adjusted by changing the geometry of each of the links, the mass of the board, and the power of the motor. Additionally, changing the position of the rocker relative to the crank alters the board angle, which generates waves of different heights. To ensure that the wave generation system produced the necessary testing environment several aspects

needed to be considered, including the water displacement and wave height, the geometry of the linkages, the power requirements and motor selection, and the stresses exerted at the joints. Other considerations were made to determine the proper features of the test tank, including material selection and placement of electronic equipment.

3.3.1. Wave Height Calculations

The first step to create the proper testing conditions was to calculate the wave heights that could be produced by this system. Since waves are produced by the movement of the board, the volume of water that the board displaces should be equal to the volume of the wave. Making the mathematical assumption that the cross-sectional area of ocean waves can be modelled as two dimensional sine waves, a sine function was generated. Knowing that the wave period is one wave every three seconds and that there is no horizontal or vertical shift, the amplitude, which in this case equals wave height (h_{wave}), is left as the only unknown.

$$h_{wave} * \sin\left(\frac{2\pi}{3}t\right)$$

Integrating this equation over the time interval of one wave results in the cross-sectional area of the wave. Taking this area and multiplying it by the width of the test tank gives the volume of the wave. Since the volume of displaced water is equal to the volume of the wave, the wave height can be easily calculated. To calculate this unknown, the cross sectional area of displaced water was divided by the integral of the wave during half of its time interval. This resulted in the following equation:

$$h_{wave} = \frac{Area}{\int_0^{1.5} \sin\left(\frac{2\pi}{3}t\right) in\ dt}$$

In this equation “Area” corresponds to the cross-sectional area of the displaced water, while the integral represents the wave. Dividing the area of the displaced water by the wave, the height of the wave can be obtained. Since one wave should occur every three seconds in order to model real ocean waves, the wave will reach its maximum height at 1.5 seconds

Unfortunately, this equation proves to be inaccurate due to velocity differences between the board and the water. As the board moves forward, the water travels away from the board at a faster velocity, meaning that some of the water volume is lost in the process. To achieve the most accurate measurement, iterative calculations were performed in a variable experiment study to determine when the board velocity approached the wave velocity. For the variable experiment study, the board height,

diameter of the cam, initial angle of the board, and height of the water were all considered. By changing these input parameters, the board velocity, wave velocity and area of displaced water were able to be determined for each scenario. A diagram relating the water height, board height, and initial and final board angles can be seen below.

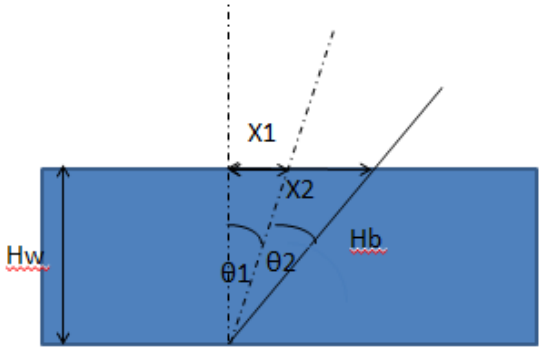

Figure 10 Diagram for Wave Height Determination

In this visual representation h_w,h_b, θ_1, θ_2, x_1, x_2 represent the height of the water, height of the board, initial angle of the board, final angle of the board, initial x direction distance, and final x direction distance, respectively. Out of these values, the height of the water, height of the board, and initial angle are all input variables. θ_2 is a calculated value that comes directly from the cam diameter (d) and board height. Since h_b, h_w, cam diameter (d), and θ_1 are all dependent variables, θ_2 can be calculated by:

$$a^2 = b^2 + c^2 - 2bc * cosA$$

$$d^2 = h_b^2 + h_b^2 - 2h_b^2 * \cos(\theta_2)$$

$$\cos(\theta_2) = \frac{(2h_b^2 - d^2)}{2h_b^2}$$

$$(\theta_2) = \cos^{-1}\frac{(2h_b^2 - d^2)}{2h_b^2}$$

Additionally, x_1 and x_2 can be determined by:

$$x_1 = h_w \tan(\theta_1)$$

$$x_2 = h_w \tan(\theta_2)$$

Knowing, x_1, x_2, h_w, θ_1, and θ_2, the area of the displaced water can be calculated:

$$Area = \frac{1}{2} * h_w^2(\tan(\theta_1 + \theta_2) - \tan(\theta_1))$$

Additional parameters that were determined through this study included the board velocity and wave velocity. Board velocity was determined by dividing the throw distance, which is the entire distance the

board travels in the positive x direction, by half of the time period (1.5 seconds). Wave velocity was calculated by using the formula:

$$v_{wave} = \sqrt{\frac{2g(throw\ distance)}{2\pi}}$$

Varying one input variable at a time, while keeping the others constant, resulted in finding the specifications that resulted in the smallest difference in wave versus board velocity. From this analysis it was determined that in order to keep the velocity difference small, a larger board height, smaller cam diameter, lower initial board angle, and lower water height were essential. Although a lower water height kept the velocity difference small, a water height of at least 12 inches was necessary in order to neglect frictional forces from the bottom of the tank. Ultimately, it was determined that a board height of 24 inches, cam diameter of 2 inches, initial board angle of 0 degrees, and a water height of 12 inches would give the smallest difference in velocities. Although these would result in a small velocity difference, the board and wave velocity still would not be equal, meaning that some of the displaced water volume would still be lost in the process. To account for this loss in volume, an assumption was made that 25% of the water that was displaced would be transmitted to the wave volume. This assumption was made based off of a velocity difference of approximately 10.4 inches/sec. From this assumption, it was calculated that the wave height would be approximately 2.5 inches.

3.3.2. Geometry of Four Bar Mechanism

After some of the parameters were determined to achieve the desired wave height, the appropriate geometry of the four bar mechanism was developed. Measurements that needed to be specified included where the crank should be placed relative to the rocker and how long the connecting rod should extend. These geometric specifications were able to be determined using data from the variable experiment study as well as Linkages software by Norton.

In order to determine the appropriate geometry it was essential to understand the necessary constraints. From the wave height calculations it was determined that the board height, cam diameter, water height, and initial start angle must be 24 inches, 2 inches, 12 inches, and 0 degrees, respectively. From these input parameters, it was also determined that the board would rotate approximately 5 degrees (θ_2) in order to achieve the desired wave height. Using these dimensions, a model of the four bar linkage was developed in Linkages.

Iterative attempts were completed to find which rod lengths and crank versus rocker dimensions resulted in the correct initial and final board angles. To complete this analysis, the board and

cam lengths remained constant, while the x and y distances of the rocker in comparison to the crank were adjusted. As those distances were changed, the rod length needed to be adjusted accordingly. It was essential to have the board begin at a 90 degree angle with respect to the bottom of the tank and finish its forward movement at an angle of approximately 85 degrees. After several attempts were completed, it was shown that in order to achieve an approximate 5 degree pivot angle with a board of 24 inches, the rod must be 19.5 inches, and the center of the cam and bottom of the board must be located 18 inches apart in the x direction and 28 inches apart in the y direction. A sketch including these measurements can be seen below:

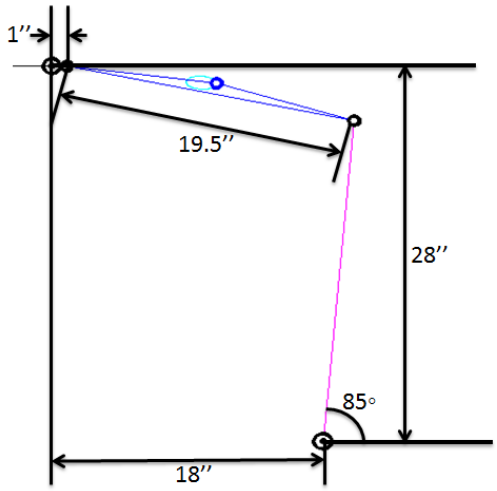

Figure 11 Wave Generator Geometry

Using this software, the wave generating mechanism was set up according to this geometry.

3.3.3. Power Requirements & Motor Preparation

In addition to the proper geometry for setup as well as the estimated wave heights, the power requirements for the system also needed to be calculated. To generate the required waves, a motor was needed that could push the water at the desired speed. Since power can be calculated by multiplying torque by angular velocity, and the angular velocity was previously determined to be 20 RPM based off the knowledge that one wave should occur every three seconds, the torque acting on the motor was the only variable that needed to be defined. To find this value, the kinematics of the wave generation system were analyzed by starting with the forces exerted on the board and then continuing upwards through the entire wave generating mechanism.

The board was the first piece to be analyzed because of its direct interaction with the water. Looking at a free-body diagram of the board (Figure 12), the forces that act on it include the force of the rod in the x direction as well as the force of the water and weight of the board.

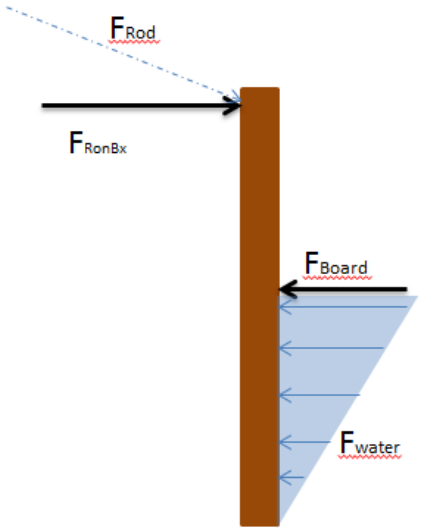

Figure 12 FBD of Board

The force of the rod in the x direction was determined by understanding that the rod creates torque equal and opposite the board and water about the hinge. To determine the torque, and thereby find the force that the rod exerted, calculations for the torque from the board weight and water were completed. The torque of the board was calculated by the following steps, in which "r" is half the length of the board (12 inches), "Θ" is the angle that the board rotates (5 degrees), "t" is half of the time interval (1.5 seconds), and "m_b" is the mass of the board (4 kg). From these calculations it can be seen that the torque from the board is approximately 0.014J.

Torque from Board

$$vel_{ib} = 0\frac{in}{s}$$

$$vel_{fb} = \frac{r\theta}{t} = 0.667\frac{in}{s}$$

$$a_b = \frac{(vel_{fb} - vel_{ib})}{t} = 0.445\frac{in}{s^2}$$

$$F_b = m_b a_b = 0.045\ N$$

$$\tau_b = F_b r = 0.014\ J$$

Calculating the torque from the water was more complex for multiple reasons; the first being that there was water on both sides of the board, and the second being that the torque of the water varies with different distances from the hinge. To account for the water being on both sides of the board, the force of the water was doubled, and to account for the varying torque, an integral was computed over the varying water heights (0-12 in). The mass of the water was determined by

multiplying the density times the volume of water that was displaced. The steps for those calculations can be seen below. In the calculations ρ, dA_b, h, Θ, t, and w_{tank}, represent water density, changing cross-sectional area, water height, board angle, time elapsed, and width of the tank, respectively.

Torque from Water

$$dF = 2 * \rho * A_b * \frac{h^2 * \theta^2}{t^2}$$

$$\tau_{H_2O} = \int_0^{12} h\, dF$$

$$\tau_{H_2O} = \int_{0in}^{12in} \left(2\rho \frac{h^3\theta^2}{t^2} w_{tank}\right) dh = 0.012\, J$$

Knowing the torque of the water and board was equal and opposite the torque of the rod, the force that the rod exerts in the x direction was determined by adding together the torque from the water and board and then dividing by the distance of the rod to the hinge (24 inches). From that calculation, it was determined that the rod exerts a force of 0.043N in the x direction, as can be seen below.

$$F_{RonBx} = \frac{\tau_b + \tau_{H_2O}}{24\ in} = 0.043N$$

The next step was to find the force that the rod exerts on the cam. Since the rod is pinned at both ends and carries no other loads, it was simplified into a two force member. The two forces acting on the rod include the force of the board and the force of the cam. When modeling a two force member, the forces are equal and opposite when they act along the centerline of the member. Knowing the force that the rod exerts on the board in the x direction, the force that the board exerts through the centerline of the rod was calculated by finding the angle that the rod makes in relationship to the horizontal. A free body diagram of the rod is shown in Figure 13.

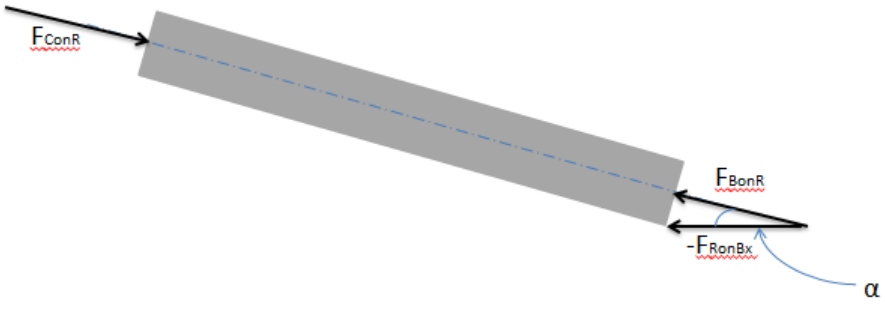

Figure 13 FBD of Rod

The angle of the rod was computed using the length of the rod, as well as the angle of the cam when the board was upright. The length of the rod was 19.5 inches, forming the hypotenuse of the triangle, while the distance in the x direction was 18 inches plus the extra x direction distance due to the 18 degree angle of the 1 inch cam. From these dimensions, it was found that the angle formed by the rod was 13.627 degrees. Knowing the angle that the rod forms, the force exerted on the rod along its centerline was determined.

Forces on the Two Force Member (Rod)

$$L_{rod} = 19.5\ in$$

$$d_x = 18\ in + \cos(18) * 1\ in = 18.951\ in$$

$$\alpha = \operatorname{acos}\left(\frac{d_x}{L_{rod}}\right) = 13.627\ deg$$

$$F_{BonR} = \frac{F_{BonRx}}{\cos(\alpha)} = -0.044N$$

$$F_{ConR} = F_{BonR} = 0.044N$$

This concluded that the force of the cam along the centerline of the rod was 0.044N.

By analyzing the cam further, the force that it exerts perpendicular to its moment arm was calculated. A free body diagram of the cam is seen in Figure 14

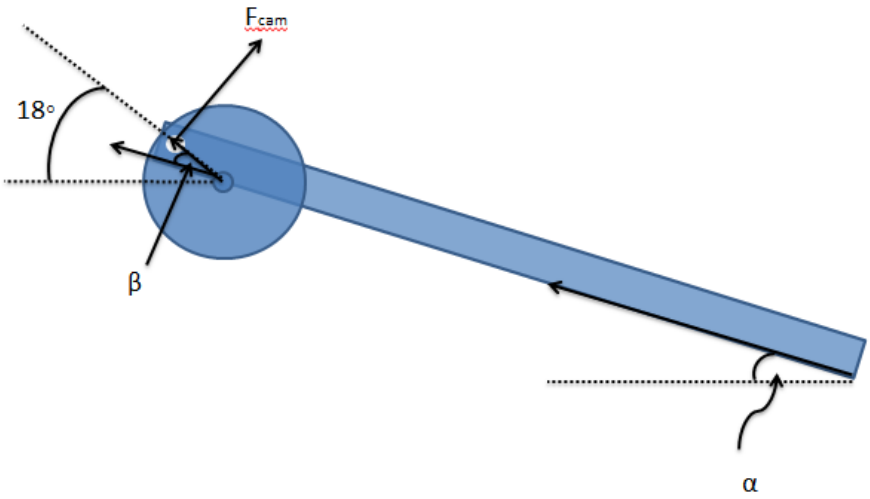

Figure 14 FBD of Cam

By determining the angle, β, and then multiplying sin(β) by the force of the cam along the centerline of the rod, the force of the cam was determined. These calculations are seen below.

$$\beta = 18 - \alpha = 4.373\ deg$$

$$F_{cam} = \sin(\beta) * F_{ConR} = 3.152 \times 10^{-3} N$$

Multiplying this force by its moment arm resulted in the torque produced by the cam. Since the moment arm in this case is the radius of the cam (1 inch), the torque was found to be $8.005X10^{-5}$ J.

In order to find the power required from the motor, the torque of the cam was multiplied by the angular velocity of the motor to give a power requirement of $1.677\ X10^{-4}$ Watts. This means that in order to produce 2 inch waves in the small scale system about one milli-watt of power was required.

After completing calculations for the power requirements, it was necessary to determine an acceptable motor for this system. A 226 Series Gearhead Motor from AM Equipment was acquired and found to produce as much at 71 Watts of mechanical power, enough for the wave generation system. The specification sheet for this particular motor can be found in Appendix A. Although this motor was capable of producing the required power, the torque exerted on the shaft from the water and board was not significantly high, therefore causing the motor to operate too fast. In order to alleviate this problem, a pulse width modulator was created in order to slow down the speed of the motor.

To slow down the motor to 20 RPM to account for wave scaling factors and a wave frequency of 20 waves per minute, different options were explored. While gears or other mechanical devices were considered, it was necessary to minimize power losses and as such use an electronic circuit. The specific circuit chosen falls in the category of a Pulse Width Modulator (PWM). The function of a PWM is to essentially act as a controllable timed on and off switch with a high frequency that turns a constant DC Voltage (such as that delivered from a car battery) into something resembling a Square Wave. Ideally a PWM can control both the frequency of the output function as well as the duty cycle, which is defined as the ratio of on and off time, or the width of the square wave Figure XYZ illustrates the variety of output functions that a PWM can produce as well as a variety of functions with differing duty cycles. The percentage values are equivalent to the duty cycle of each wave.

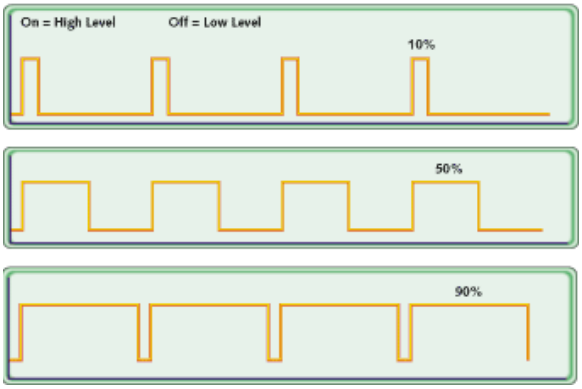

Figure 15 Variety of Duty Cycle Outputs Generated by PWM

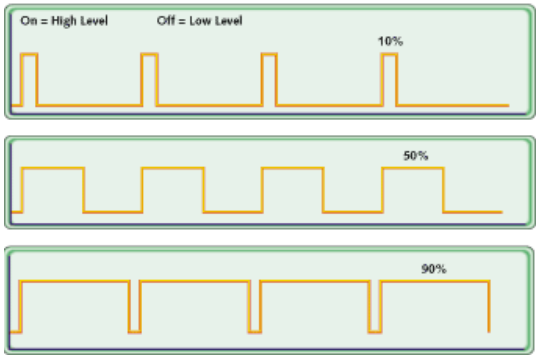

Figure 16 Circuit Diagram of Pulse Width Modulator (Jan will update this picture later)

The PWM design had to be highly controllable to account for different testing parameters, while also minimizing power losses and maximizing power output. The circuit design that was employed is pictured in Figure XYZ2. This specific circuit uses a NE555N timer as its centerpiece, two potentiometer (variable resistors) to control both the frequency and the duty cycle of the output function, two MOSFET IRF 520 switches to aid in heat dissipation and a number of protective diodes and capacitors.

After the pulse width modulator was created, the motor also need to be prepared to be used in the wave generation system. Preparation included machining a press fit linkage to the motor's shaft. After measuring the shaft dimensions, interference calculations were completed by determining the pressure and torque of the shaft within the hub of the linkage. Using an interference of 0.001 inches pressure was calculated by:

$$P = \frac{0.5\delta}{\frac{r_h}{E_o} * \left(\frac{r_o^2 + r_h^2}{r_o^2 - r_h^2} + v_o\right) + \frac{r_s}{E_i}(1 - v_i)}$$

Where r_s, r_h, r_o, δ, v_o, v_i, E_o, E_i, represent the shaft radius, inner hub radius, outer hub radius, difference between shaft radius and inner hub diameter, Poisson's ratio of the hub material (6061 Al), Poisson's ratio of the shaft material (steel), the elastic modulus of the hub, and the elastic modulus of the shaft, respectively. The torque was calculated by:

$$T = 2\pi r_s^2 \mu P l$$

Where μ represents the coefficient of friction between the shaft and hub, and l represents the length of contact between the two interfaces. From the pressure and torque calculations, it was found that an interference of 0.001 inches was sufficient to create a proper press fit. A model of the linkage, which can be seen below, was designed taking into account the necessary interference.

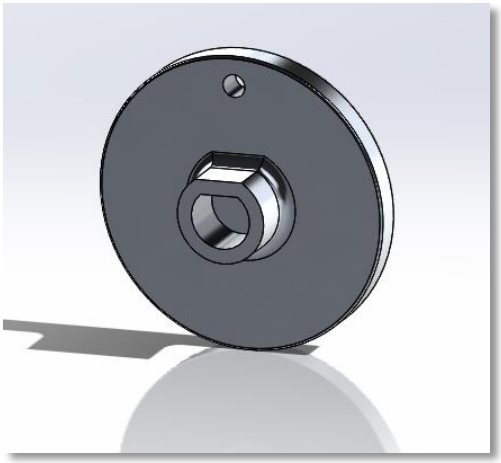

Figure 17 Motor Cam

Once the model was designed, it was then manufactured using 6061 aluminum at the machine shops in Washburn. The stock metal was first shaved down to the proper dimensions in the lathe, and then the mill was used to form the drilling operations. The linkage was then press fit to the motor shaft by heating up the metal and then applying force. Once cooled, the linkage was securely fastened to the motor shaft as seen in Figure 18, thereby preparing the motor for wave generation.

Figure 18 Motor with Cam Attached

3.3.4. Stresses Exerted at the Joints

Along with finding the power requirements of the system, another important factor to consider was the stresses exerted at all the joints. In the wave generation system there are four major areas of stress concentration; the two hinges connecting the board to the test tank, the pin connecting the rod to the board, and the pin connecting the rod to the cam. Each of these stress concentrators were analyzed to ensure that they would be capable of handling the necessary loading conditions. The first area that was analyzed included the hinges connecting the board to the bottom of the tank. A schematic with the loading conditions can be seen below:

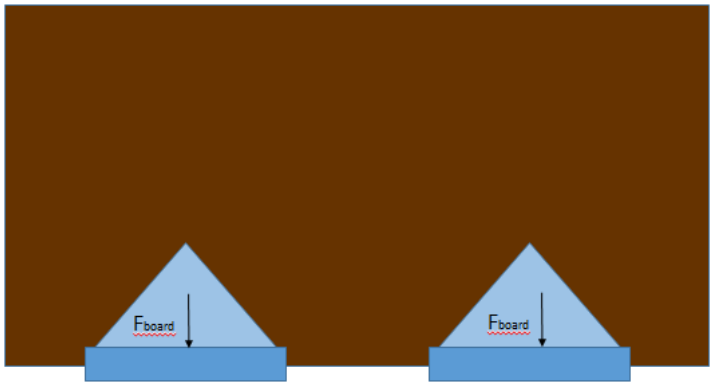

Figure 19 Hinges Connecting Board to Test Tank

The only force that is exerted on the hinges is the force of the board. Since the hinges have a 0.5 inch diameter and the force of the board can be split amongst the two hinges (assuming that the hinges are positioned symmetrically about the board), the shear stress exerted on each hinge can be calculated by:

Shear Stress on Hinges Connecting Board to Test Tank

$$D_{hinge} = 0.5\ in$$

$$Area_{hinge} = \pi\left(\frac{D_{hinge}}{2}\right)^2 = 1.267 \times 10^{-4} m^2$$

$$\tau_{hinge} = \frac{m_b * g}{2 * Area_{hinge}} = 1.548 \times 10^5 Pa$$

Each hinge experiences a shear stress of 0.1548MPa. This means that they will be more than capable of handling the stress exerted on them since they are made from steel, which has a shear strength ranging from 165-1130 MPa.

The next joint that was taken into consideration included the pin connecting the rod to the board. The forces exerted on this pin included the force of the board as well as the force of the rod. Figure 20 shows a free body diagram of this joint.

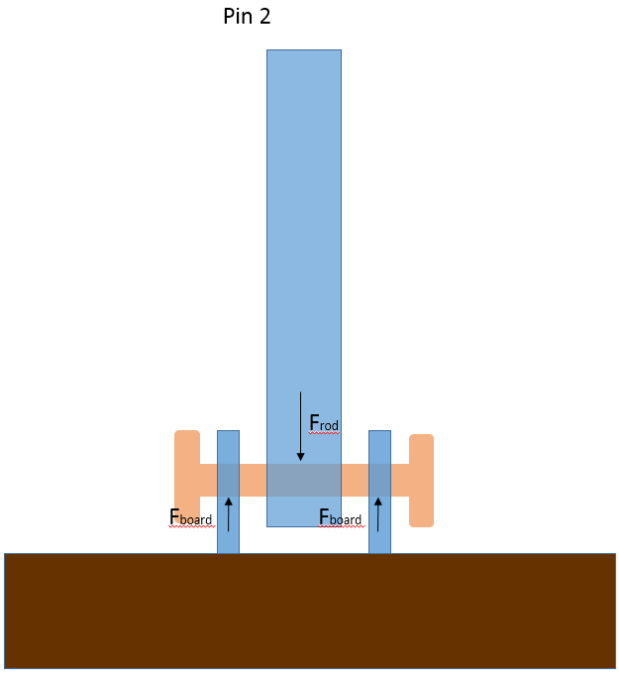

Figure 20 Pin Connecting Rod to Board

Since the board is connected in two different locations, the pin experiences double shear, meaning that the stress is cut in half. Calculations for the shear stress exerted on this pin can be seen below:

Shear Stress on Pin Connecting Board and Rod

$$D_{pin2} = 0.5\ in$$

$$Area_{pin2} = \pi\left(\frac{D_{pin2}}{2}\right)^2 = 1.267 \times 10^{-4} m^2$$

$$\tau_{pin2} = \frac{-F_{BonR}}{2 * Area_{pin2}} = 163.16\ Pa$$

The shear stress at pin 2 is only 163.16 Pa. Since pin 2 is also made from steel, there is no concern about the pin experiencing failure in this environment.

The final joint that was analyzed was the pin connecting the cam to the rod. As seen in Figure 21, the forces that act on this pin include the force of the cam and the force of the rod, which were previously determined to be equal and opposite.

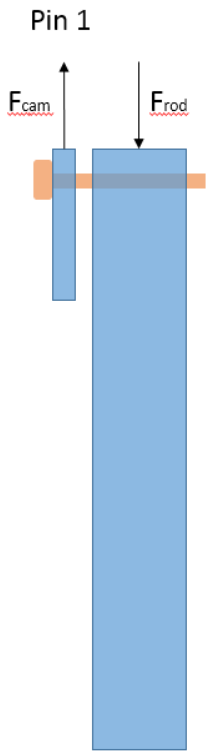

Figure 21 Pin Connecting Cam to Rod

In order to determine the shear stress acting on pin 1, the force exerted on the pin was divided by the cross-sectional area of the pin. The pin used in the system is approximately 0.190 inches in diameter. The calculations for the shear stress can be seen below:

Shear Stress on Pin Connecting Cam and Rod

$$D_{pin1} = 0.19\ in$$

$$Area_{pin1} = \pi\left(\frac{D_{pin1}}{2}\right)^2 = 1.829 \times 10^{-5} m^2$$

$$\tau_{pin1} = \frac{F_{ConR}}{Area_{pin1}} = 2.26 \times 10^3\ Pa$$

The shear stress acting on pin 1 is 2.26 kPa. Since this pin is also made out of steel, it will be able to handle the testing environment. This shows how all areas of stress concentration will remain intact.

3.3.5. Other Considerations

Other important components of the wave generation system included its overall features. The system was placed in a large wooden test tank. The test tank was 8 feet long, 3 feet wide, and 2 feet deep. In order to keep the tank water proof, it was coated with a water resistant layer and then sprayed with a rubber sealant along all the edges. Additionally, the tank was made with no legs so there would

not be concentrated areas of stress. Wooden supports were placed underneath and along the edges of the tank for extra stability and security.

It was also very essential to ensure that the electrical components did not interact with the water. To do this, the motor was mounted four inches above the top of the test tank by means of a metal slotted angle. A U-clamp tightly secured the motor to the metal angle. Additionally, a 12 Volt car battery was placed on the ground behind the motor. The battery was covered and shielded by a plastic tarp. The pulse width modulator was placed on a flat surface next to test tank, ensuring that it would not fall into the filled tank. The necessary precautions were taken in order to keep the team safe as well as keep the equipment from being damaged.

3.4 Design of Overtopping Device

By combining the desirable aspects of Wave Dragon and SSG as discussed in Chapter 2, a new overtopping device was designed as shown below in Figure 22. The device consists of three tiers of reservoirs that empty into each other. In the actual device a multi-stage turbine would connect each tier, converting the stored potential energy into power, however, due to the small scale nature of this prototype, the turbine was omitted. The device was attached to the test tank to mimic anchoring and avoid movement during wave simulations and testing. It should be able to continuously operate, as waves will constantly be entering at least one of these three tiers due to the slight bottleneck design. Consistent operation will allow the overtopping device to reach higher efficiencies than other systems.

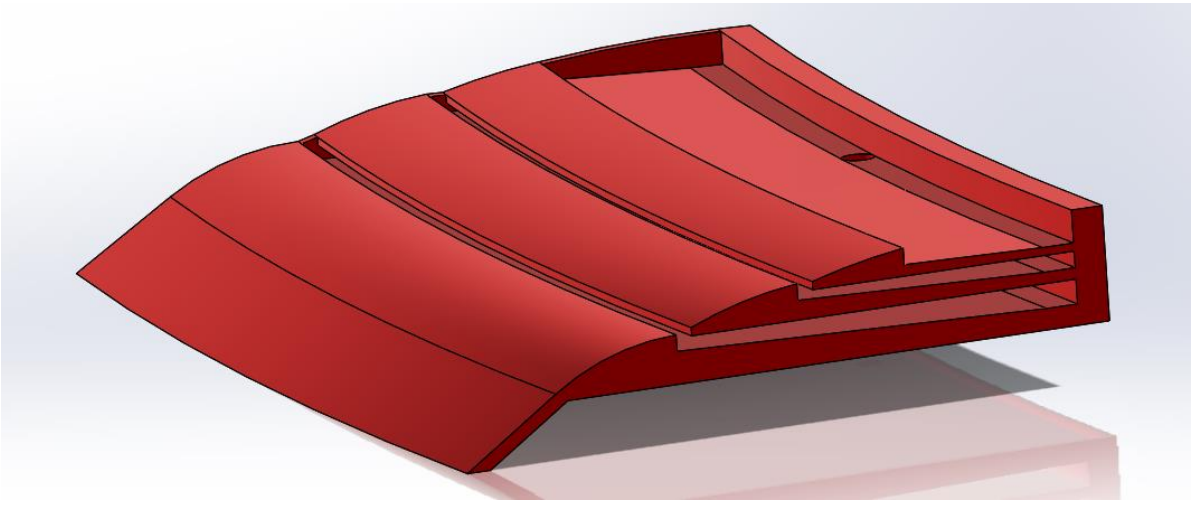

Figure 22: Overtopping Prototype

An actual full-scale design would incorporate wave reflectors on each side in order to maximize the amount of waves that are captured. For the purpose of this project, the wave reflectors were omitted due to size limitations of the test tank.

This particular prototype can be broken into three main design categories that are crucial to its functionality: tier design, ramp design, and tier drain system.

The prototype was designed so that the tiers optimally function under 2 inch waves. As mentioned previously in chapter 3.2.: tier one has a relative height of 0.6 times the wave height, tier two has a relative height of the wave height, and tier three has a relative height of 1.2 times the wave height. Each tier is also tapered so that the water is forced to flow towards the back of the device where it is outputted to the draining system. The bottom of the prototype is designed so that the device is able to float above the water. To do this, the prototype is shelled out at the bottom so that there is a pocket of air in between the prototype and the surface of the water. Not only does this allow the device to float, but it also allows water flow out of tier 1. Without a pocket of air there would be no potential energy, restricting any volume of water from flowing out of tier 1.

Another important part of the device design is the ramp. A wave is felt up to half its height under water, therefore the bottom ramp, leading to tier 1, is designed to account for the felt wave height. Since the wave will break on the prototype, there will not be any disturbances under the device. The ramps leading to the higher tiers are overlapped such that if the wave does not make it all the way up the ramp, it will fall back down into the previous tier. This is shown in the image below:

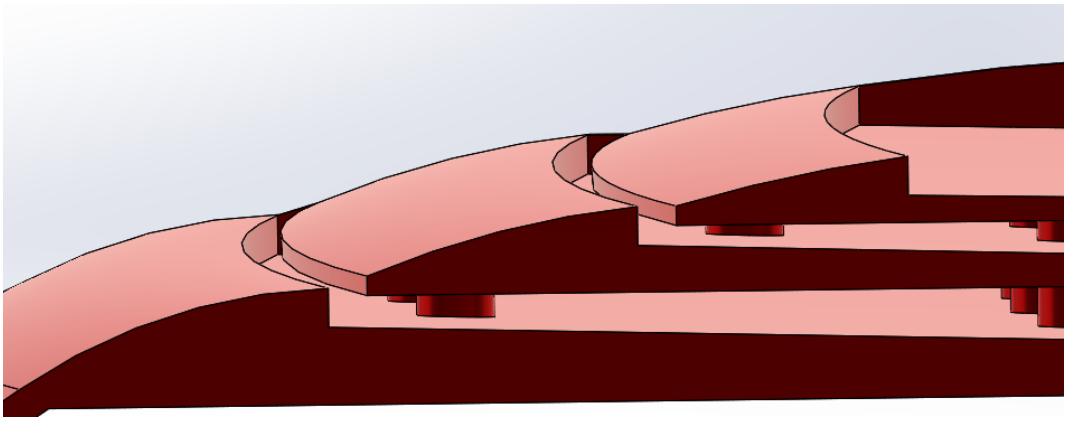

Figure 23: Ramp Design

Producing a turbine for this prototype was not possible due to budget and size constraints; therefore, in order to simulate the actual output of a turbine, the theoretical power output was calculated by measuring the volume of water that was captured. To do this, a hole large enough to drain the volume of one wave before the next wave enters, was created in the prototype, extending through all 3 tiers. The tiers were designed with enough depth in order to hold more than one wave's volume. The reason for designing the prototype in this way was to maintain a constant head. By

maintaining constant head, the prototype can fulfill both the minimum head requirement and constant operation for the turbines.

A tubing mechanism was developed, enabling water to be captured from one tier while closing off the other two. To do this a pipe fitting was inserted in the hole that extends through the bottom of all three tiers. At each tier level, a hole was cut in the pipe fitting allowing water to flow out of all three tiers simultaneously. A smaller pipe that fits tightly inside of the pipe fitting was broken into six evenly spaced sections. Each odd numbered section was designed to drain just one tier specifically. For example, when Section 1 is aligned with the holes of the outer fitting, tier 3 is able to drain while the other two remain shut. Section 3 and 5 are able to drain only tier 2 and 1 respectively. Each even numbered section is designed to block off all tiers. These sections have two purposes. One purpose is to stop draining a tier successfully without opening the hole of another tier. The second purpose is so the optimization of maximum head is possible before opening the channel of a tier to drain. The figure below shows section one of the tier drain system.

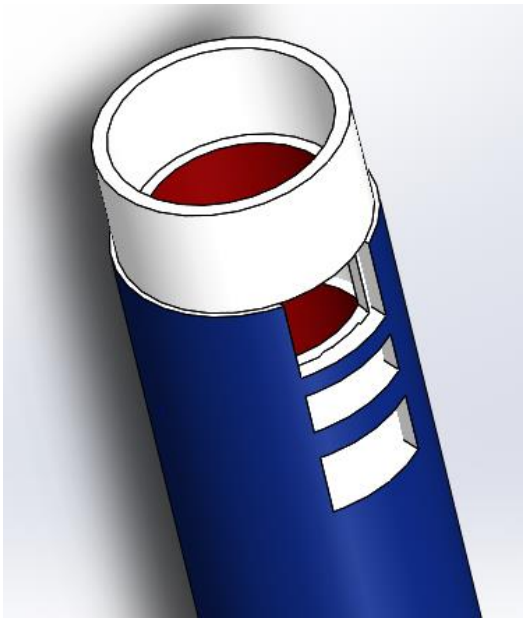

Figure 24: Tier Drain System

3.5 Construction of Test Tank and Device

3.5.1. Test Tank Construction

The wave tank was constructed for the purpose of testing the wave energy converter while simulating specified wave characteristics, such as the deep-water waves. The wave tank was constructed from 2x6's and ¾" plywood. The tank is illustrated in the SolidWorks drawing and model below.

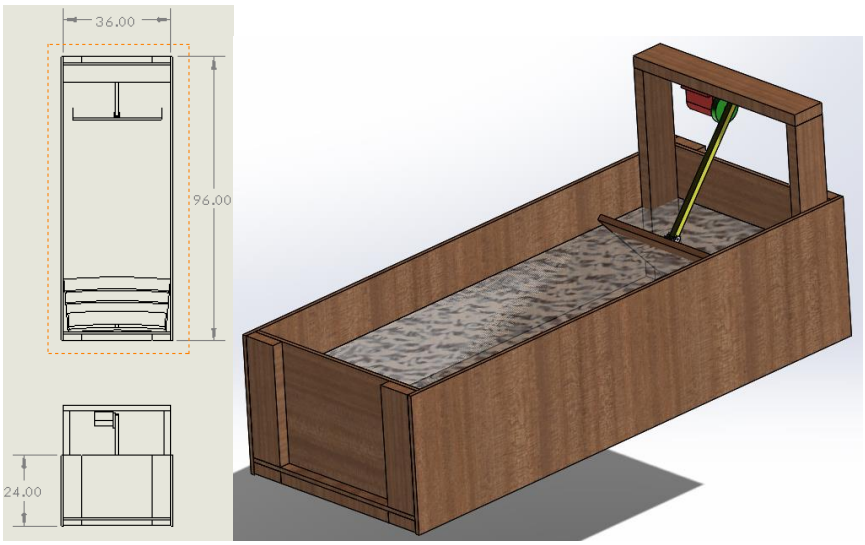

Figure 25 SolidWords Drawing and Model of Wave Tank

Construction began by cutting all pieces to the proper dimensions: two 8'x2' side pieces, two 3'x2' pieces for the front and back, and one 3'x8' bottom piece. Once all pieces were cut, the frame was built by attaching the 2x6's with supporting joints at the corners for added strength. The plywood was then added to this frame for enclosure of the tank. Additionally, supports were added at the center of the tank to prevent collapsing under a heavy load of water. In order to ensure the waterproof interior, latex was coated along the inside with rubber lined along the seams of the tank. The exploded view below illustrates the assembly process of the wave tank.

Figure 26 Exploded View and Final Construction of the Wave Tank

3.5.2. Device Construction

The initial design of each tier for the wave energy converter involved the manufacturing of large sheets of plastic either to be cut to size or 3D printed. Both of these options proved infeasible due to high expenses and limited machine access. In order to utilize the resources available for manufacturing, each tier was broken into 3.5" wide segments that could be easily machined. To achieve the desired

slope across the entire device, the thickness at the front and back of each tier was determined and a continuous slope was cut across each segment to form a continuously flowing piece. The continuous slope was created by machining grooves in a small metal block at the calculated slope and resting each board on the block to be machined. Due to the 3’ length of the board, the milling tool experienced a great deal of chatter during the cutting operation. To ensure a smooth surface finish to reduce frictional effects, a metal rod was taped to the underside of the board to add mass and minimize chatter. This same process was utilized to create all three tiers of the device.

Once all of the slopes were machined, the tiers required assembly of the 3.5” wide segments using a technique called biscuit jointing. Biscuit jointing involves a process of cutting small slots in the material and inserting wooden biscuits that hold the pieces together.

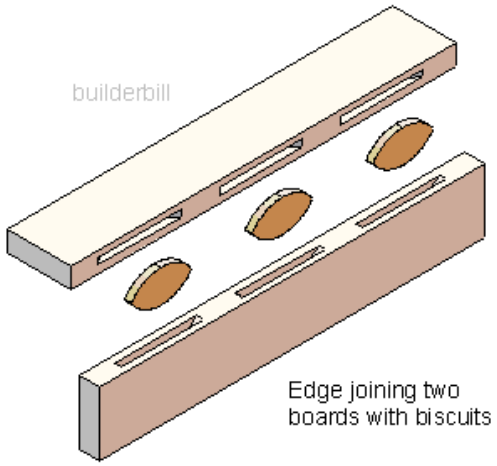

Figure 27 Biscuit Joint Exploded View (Biscuit, n.d.)

Biscuit jointing was used on each of the three tiers consisting of five, four, and three segments for tiers one, two, and three respectively. The tiers were glued with PVC cement and clamped together to allow for proper setting and drying of the tiers.

Figure 28 Clamped Tier 1 to Allow Proper Setting of Biscuit Joints

Following the assembly of the tiers, the sideboards and backboards were constructed to support the system. The cuts were easily achieved by creating dxf files exported to the CNC mills which quickly cut the tier cross-section into the sideboards.

Figure 29 Cross-Section of the Sideboards

The tier slots were cut .375” deep into the PVC trim to provide as much support as possible for each reservoir without compromising the integrity of the sideboards. The two sideboards were created as mirror images so as to hold the tiers in their respective slots.

Finally, the backboard was created to close off each reservoir and provide extra structural support for each tier. The backboard was created in a similar fashion to the sideboards, using CNC milling which was established by the SolidWorks image illustrated below.

Figure 30 SolidWords Drawing of the Backboard

The simplistic design for the backboard allows the back to sit on the bottom tier so as to maximize support from this level and provides slots for the remaining top two tiers cut at the same depth as the sideboards at .375”. Concluding the machining of the tiers, sideboards, and backboard, the pieces were all assembled using PVC cement and clamped in place for proper setting.

3.5.3. Assembly of Testing Unit

Upon completion of machining the wave energy converter, additional assembly was required to account for the testing procedure. To provide a means of capturing and measuring volume, an expansion adapter tube was utilized in the device. A hole of diameter 2.81” was machined in the center of the back segment of each tier to produce a continuous hole throughout the device. To accommodate the flow of water through each tier, CNC milling was used to create openings for each level of the expansion adapter as shown below.

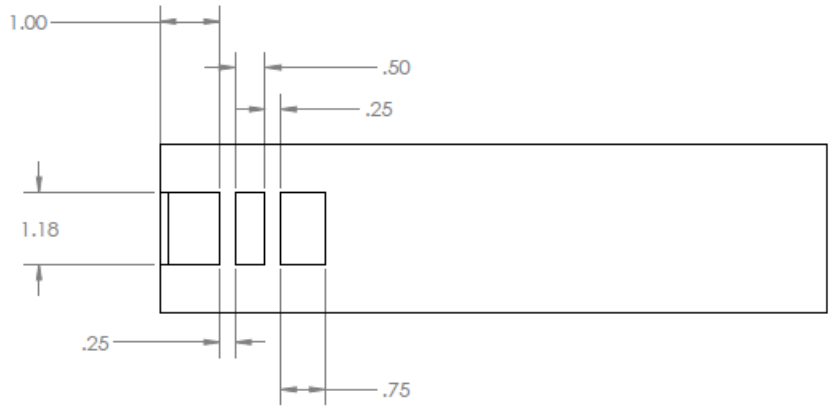

Figure 31 Drawing of Expansion Adapter for Water Collection

Each opening lines up perfectly with the three tiers and provides a tight seal using PVC cement to seal and lock the expansion adapter in place. Furthermore, the inner tube of the expansion adapter was altered to close off flow to all but a single tier at a time. In doing so, the volume can be measured from each tier to determine efficiency of the multiple levels. By removing the inner tube altogether, the entire device can be tested at once in terms of flow and volume capture. The design of the inner tube relies on the sealing off of two tiers at any given time and therefore, the openings occur at 120° apart from one another as is demonstrated below.

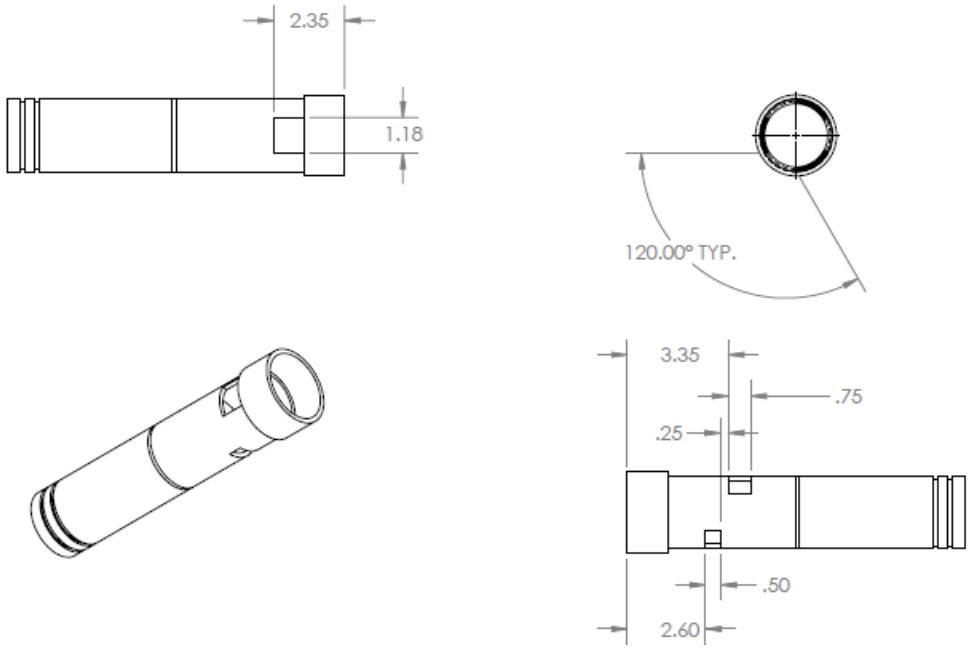

Figure 32 Inner Tube Design for Testing Different Tiers

To achieve proper sealing for each tier, O-ring grooves were cut directly below each opening using a CNC lathe. Therefore, the finished inner tube design functions with offset openings to allow flow through one tier at a time and watertight O-ring seals for each tier.

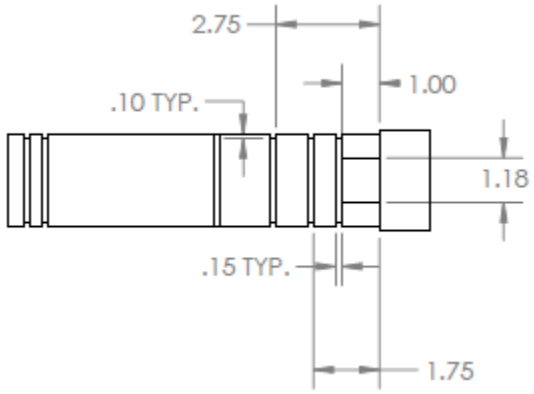

Figure 33 Finalized Inner Tube Design with O-Rings

The final construction steps required the implementation of the wave energy converter into the testing wave tank. To accomplish this, a reduction hose was required to decrease the diameter of the expansion adapter for proper fitting of a hose. The reduction hose was hose clamped to the expansion adapter. This reduction hose was then PVC cemented to a small adapter providing an outlet for a 2" OD tube. An elbow fitting was installed to slope the tube out of the bottom of the device and through a hole in the side of a tank. Large amounts of expansive rubber adhesive and caulk were applied to the boundary of the tube to ensure the tank to be watertight. Lastly, supporting boards were attached at a height of 12" where the device will rest during testing. The support boards act as a stabilizing measure to prevent extensive motion of the device while testing is taking place. The final assembly of the device with the tank is illustrated below.

3.6 Testing and Data Collection

Testing of the device was completed over the course of one day to limit any variable changes. Once the tank was filled with water to a height of 12 inches, we could begin our testing. The procedure for testing involved running the wave generator for a cycle of 60 waves, and directly measuring the volume output over the course of those 60 waves. To account for the time it took the wave generator to reach steady- state wave generation, we began collection and measurement of water only once the waves had reached a height of 2-2.5 inches. We ran a number of different tests, including the water collected by the entire device over a 60 wave cycle, the water collected by each different tier during a 60 wave cycle, and the empting time of each tier. Our raw data results are presented in the table below

Raw Data			
	Trial 1 (lb)	Trial 2 (lb)	Avg. (lb)
Tier 1	26	22	24
Tier 2	6	5	5.5
Tier 3	0	0	0

Table 3: Raw Collected Data

From our Raw Data Results it is clear to see that no water entered the top tier, and all the water collection occurred in the first and second tiers (from the bottom). The raw data also showed that our water collection was equal whether we plugged up the tiers one by one and totaled the result, or ran the prototype with all tiers operating. Below is an image of our prototype during operation of our tests.

Figure 34 Image of Prototype Testing

3.7 Analysis

In order to analyze this data it was first important to determine the Volumetric Flow Rate, and the theoretical output of the prototype before scaling it up to a real world application and dimension. While the raw data was in an imperial measurement of mass, we converted that to mass in SI units, and then using the density of the water, calculated the volume collected in each trial. The final step was to determine the Volumetric Flow Rate through the prototype. In order to compute the Flow Rate we calculated that we ran the test for a cycle of 60 waves, which at 20 rpm (our scaled down time factor) provides a total of 180 seconds. All these calculations are recorded in the table below.

Calculated Data				
Avg. (lb)	Avg. (kg)	Avg. (m^3)	Time Period (s)	Volumetric Flow Rate (m^3/s)
24.00	10.89	1.09E-02	180.00	6.05E-05
5.50	2.49	2.49E-03	180.00	1.39E-05
0.00	0.00	0.00E+00	180.00	0.00E+00

Table 4: Volumetric Flow Rate Calculations

The next portion of calculations to be carried out regards the scaling up of the prototype's power output. The head of each tier was determined from the CAD drawings of the prototype. The calculated power output of the prototype was determined using the following formula, where V is the Volumetric Flow Rate, ρ is the density of water, g is the acceleration of gravity, h is the head, and η is the efficiency (estimated at 90% from existing prototypes).

$$P = V * \rho * g * h * \eta$$

The next step was to determine the Power of Wave front or the power output per width of device. This was simply done by diving our Calculated Power by the width of our device (3 feet = 0.914 m). Finally, to scale-up to the Power Output in order to compare it to existing devices, we used the Froude Scaling Factor which was determined by the prototype's scale of 1:20 and the Power Factor to the power of 3.5 (see Table 1). This provided the result that our prototype, if scaled up to an environment of 1 meter waves, would produce about 337.6 W/m of the device. This is highly comparable to real world results such as the Wave Dragon which produces 400W/m of the device in similar conditions and scaling.

	Volumetric Flow Rate (m^3/s)	Head (m)	Calculated Power (W)	Power of Wavefront (W/m)	Scaled-up Power of Wavefront for 1 meter waves (W/m)
Tier 1	6.05E-05	1.27E-02	6.77E-03	7.41E-03	250.74
Tier 2	1.39E-05	1.92E-02	2.35E-03	2.57E-03	86.87
Total	7.43E-05	3.19E-02	9.12E-03	9.98E-03	337.61

Table 5: Scaled-up Power Calculations for 1 meter waves

3.8 Recommendations

The recommendations concerning our prototype and tank testing includes both modification to the wave generation device as well as the prototype. Concerning the wave generation device, it would be highly recommended to modify the Cam design. It was difficult to simulate the correct wave frequency without sacrificing wave height, as such a future recommendation would be to create a CAM

with a 5:1 forward, backward ratio such that the “push” of the paddle would create a wave within half a second, and the pull portion would take 2.5 seconds, resulting in a total period of 3 seconds, or 20 rpm, as prescribed by the Froude Scaling Factors.

The second recommendation would be to slightly redesign the height and lips of the tiers such that less water losses occurred and the top tier could be utilized during testing. However, if the first recommendation is made concerning the wave generation device, there is potential that the top tier would be utilized due to the waves having a higher forward kinetic energy, and therefore would be able to reach the topmost tier.

3.9 Conclusion

Renewable Energy Sources are an increasingly popular way of generating energy, and few are as reliable and constant as the energy provided by the ocean, specifically wave energy. While there continue to be many designs for devices that produce power through waves, overtopping devices continue to be one of the most successful technologies available. The scope of this project involved combining two existing overtopping technologies to determine if a better solution could be created. It combined the multiple tier system in the Sea Slot Cone Generator and the open water design of the wave dragon. The purpose of the project was to develop a device and prototype that could be comparable to current technologies in the field, and was successfully obtained.

References

Alamian, R., Shafaghat, R., Miri, S.J., Yazdanshenas, N., Shakeri, M. (2014). Evaluation of Technologies for Harvesting Wave Energy in Caspian Sea. *Renewable and Sustainable Energy Reviews,* 32, 468-476.

Bedard, Roger. "Offshore Wave Power Feasibility Demonstration Project." 2005.

Biscuit Joint. (n.d.). Retrieved March 1, 2015, from http://www.builderbill-diy-help.com/biscuit-joint.html

Emay, L. "Energy and the Environment-A Coastal Perspective." 22 May 2010. unc.edu. 16 October 2014 <http://coastalenergyandenvironment.web.unc.edu/ocean-energy-generating-technologies/wave-energy/oscillating-water-column/>.

Esteban, M., Leary, D. (2012). Current Developments & Future Prospects of Offshore Wind and Ocean Energy. *Applied Energy,* 90, 128-136.

Lockwood, Deirdre. “Harvesting Power When Freshwater Meets Salty." *CEN RSS*. 26 Nov. 2013. Web.

Natesan, A. (1994). Kinematic analysis and synthesis of four-bar mechanisms for straight line couple curves. Thesis: *Rochester Institute of Technology*

Payne, Gregory. Guidance for the experimental tank testing of wave energy converters. United Kingdom: The University of Edinburgh, 2008.

Pelamis Wave Power. 5 June 2014. 16 October 2014 <http://www.pelamiswave.com/our-projects/project/1/P2-Demonstration-at-EMEC-Orkney>.

Tester, J.W., Drake, E.M., Driscoll, M.J., Golay M.W., Peters, W.A., “Chapter 14: Ocean Wave, Tide, Current, and Thermal Energy Conversion.” *Sustainable Energy*. 2nd edition, 2012, MIT Press.

Thurman, Harold. Essentials of Oceanography. 1992.

Vicinanza, Diego, Lucia Margheritini, Jens Peter Kofoed, and Mariano Buccino. "The SSG Wave Energy Converter: Performance, Status and Recent Developments." *Energies* 5.2 (2012): 193-226.

Voorhis, R. Point Absorbers: The Technology and Innovations. 25 July 2012. 16 October 2014 <http://coastalenergyandenvironment.web.unc.edu/ocean-energy-generating-technologies/wave-energy/point-absorbers/>.

Appendix A

AM EQUIPMENT.COM

226-3003 Motor

- 26Nm stall torque actuator motor. LH
- 12V reversible (24V available upon request)
- Water resistant
- For use with sprockets and drives
- Weighs 2.7 pounds

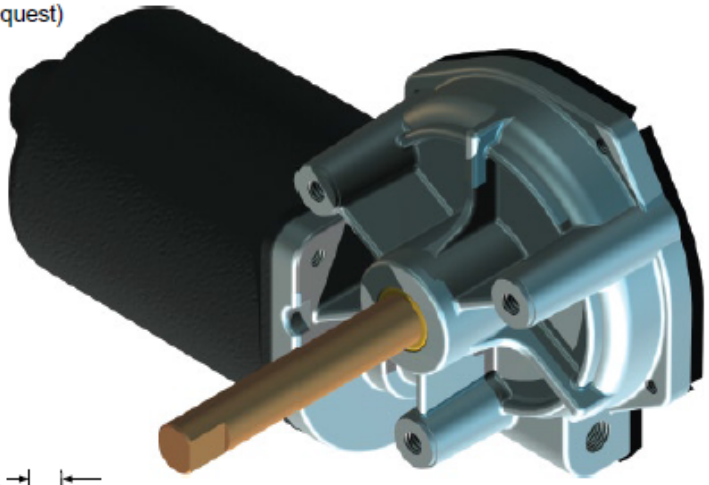

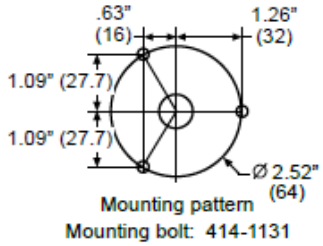

Mounting pattern
Mounting bolt: 414-1131

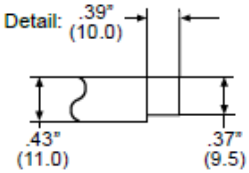

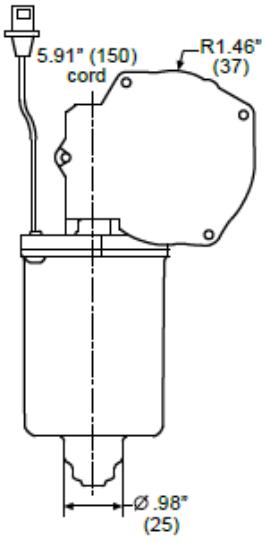

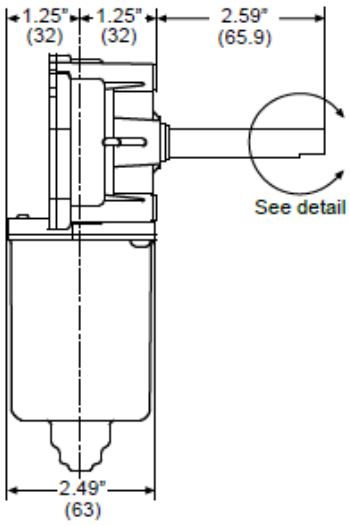

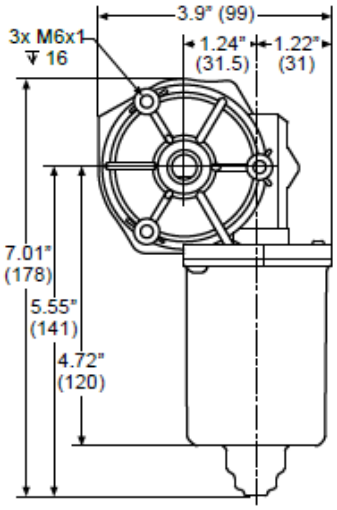

PAGE 1 OF 2

AM EQUIPMENT • P.O. BOX 790, JEFFERSON, OR 97352 • PHONE: 541-327-1546 • FAX: (541) 327-3480
ISO 9001:2008 CERTIFIED
801-1071 REV 2 02/13

AM EQUIPMENT.COM

226-3003 Motor

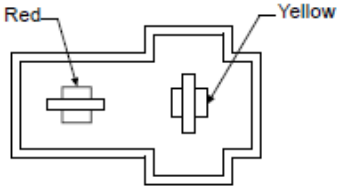

Terminal housing: 317-1057
Terminal: 317-1054
Mate terminal housing: 317-1056
Mate terminal: 317-1055

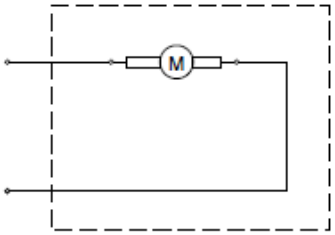

Red (+), yellow (-) = CW
Yellow (+), red (-) = CCW (preferred rotation)

Clockwise Motor Shaft Rotation		
Data Point	Data Type	Value Range
No Load	Current (A)	4.5 or less
	Speed (rpm)	95.9 - 78.5
19.5Nm	Current (A)	39.9 - 34.6
	Speed (rpm)	39.7 - 32.9
Peak Power	Power (W)	83.6 - 68.4
	Torque (Nm)	19.2 - 15.7
Nominal (Peak Efficiency)	Power (W)	44.5 nominal
	Speed (rpm)	70.2 nominal
	Current (A)	12.8 nominal
	Torque (Nm)	6.2 nominal

Counter-Clockwise Motor Shaft Rotation		
Data Point	Data Type	Value Range
No Load	Current (A)	4.5 or less
	Speed (rpm)	98.1 - 80.3
19.5Nm	Current (A)	40.9 - 34.8
	Speed (rpm)	39.4 - 32.0
Peak Power	Power (W)	84.4 - 69.1
	Torque (Nm)	18.0 - 14.8
Nominal (Peak Efficiency)	Power (W)	44.1 nominal
	Speed (rpm)	74.8 nominal
	Current (A)	11.0 nominal
	Torque (Nm)	5.8 nominal

Note:
BACKDRIVE 60Nm MINIMUM CW & CCW

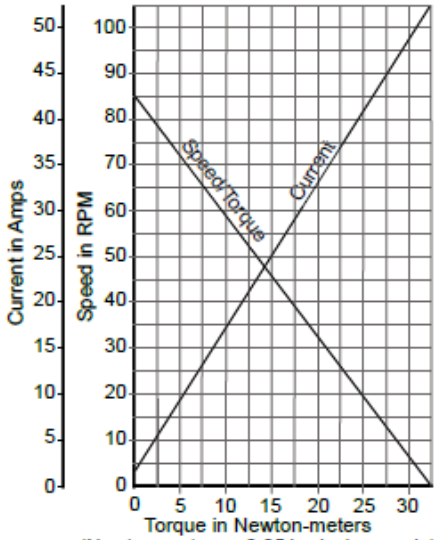

(Newton-meters x 8.851 = inch pounds)
(Newton-meters x 10.2 = kilogram meters)

AM EQUIPMENT • P.O. BOX 790, JEFFERSON, OR 97352 • PHONE: 541-327-1546 • FAX: (541) 327-3480
ISO 9001:2008 CERTIFIED
801-1071 REV 2 02/13